

AXTAR: Mission Design Concept

Paul S. Ray^a, Deepto Chakrabarty^b, Colleen A. Wilson-Hodge^c, Bernard F. Philips^a,
Ronald A. Remillard^b, Alan M. Levine^b, Kent S. Wood^a, Michael T. Wolff^a, Chul S. Gwon^a,
Tod E. Strohmayer^d, Michael Baysinger^e, Michael S. Briggs^c, Peter Capizzo^e, Leo Fabisinski^e,
Randall C. Hopkins^e, Linda S. Hornsby^e, Les Johnson^e, C. Dauphne Maples^e,
Janie H. Miernik^e, Dan Thomas^e, Gianluigi De Geronimo^f

^aSpace Science Division, Naval Research Laboratory, Washington, DC 20375, USA

^bKavli Institute for Astrophysics and Space Research, Massachusetts Institute of Technology,
Cambridge, MA 02139, USA

^cSpace Science Office, NASA Marshall Space Flight Center, Huntsville, AL 35812, USA

^dNASA Goddard Space Flight Center, Greenbelt, MD 20771, USA

^eAdvanced Concepts Office, NASA Marshall Space Flight Center, Huntsville, AL 35812, USA

^fInstrumentation Division, Brookhaven National Laboratory, Upton, NY 11973, USA

ABSTRACT

The Advanced X-ray Timing Array (AXTAR) is a mission concept for X-ray timing of compact objects that combines very large collecting area, broadband spectral coverage, high time resolution, highly flexible scheduling, and an ability to respond promptly to time-critical targets of opportunity. It is optimized for submillisecond timing of bright Galactic X-ray sources in order to study phenomena at the natural time scales of neutron star surfaces and black hole event horizons, thus probing the physics of ultradense matter, strongly curved spacetimes, and intense magnetic fields. AXTAR's main instrument, the Large Area Timing Array (LATA) is a collimated instrument with 2–50 keV coverage and over 3 square meters effective area. The LATA is made up of an array of supermodules that house 2-mm thick silicon pixel detectors. AXTAR will provide a significant improvement in effective area (a factor of 7 at 4 keV and a factor of 36 at 30 keV) over the RXTE PCA. AXTAR will also carry a sensitive Sky Monitor (SM) that acts as a trigger for pointed observations of X-ray transients in addition to providing high duty cycle monitoring of the X-ray sky. We review the science goals and technical concept for AXTAR and present results from a preliminary mission design study.

Keywords: Neutron Stars, Black Holes, X-ray Timing, Silicon Pixel Detectors, Mission Concepts

1. INTRODUCTION

The properties of ultradense matter and strongly curved spacetime and the behavior of matter and radiation in the extreme environments near compact objects are among the most fundamental problems in astrophysics. X-ray timing measurements have powerful advantages for studying these problems.¹ The X-ray band contains most of the power emitted by accreting neutron stars and black holes, and this radiation is relatively penetrating even in these complex environments. The rapid X-ray variability of these objects encodes their basic physical parameters, and interpretation of this variability is relatively straightforward for rotating or orbital origins. In many cases, the properties of the X-ray variability allow extremely precise measurements and detailed quantitative inferences. The scientific promise of X-ray timing has been spectacularly demonstrated by the success of NASA's Rossi X-ray Timing Explorer (RXTE; effective area $A_{\text{eff}} = 0.6 \text{ m}^2$; launched 1995), which has revealed an extraordinary range of previously unknown variability phenomena from neutron stars and black holes. However, redeeming that promise and exploiting these phenomena to answer fundamental astrophysical questions will require a larger-area follow-on mission. A detailed scientific case for such a mission was first explored at the conference *X-ray Timing 2003: Rossi and Beyond* in Cambridge, Massachusetts.²

In this paper we describe the Advanced X-ray Timing Array (AXTAR; see Figure 1), a new mission concept with significantly larger effective area than RXTE (see Figure 2), allowing it to exploit the phenomena discovered

Send correspondence to P.S.R. E-mail: paul.ray@nrl.navy.mil

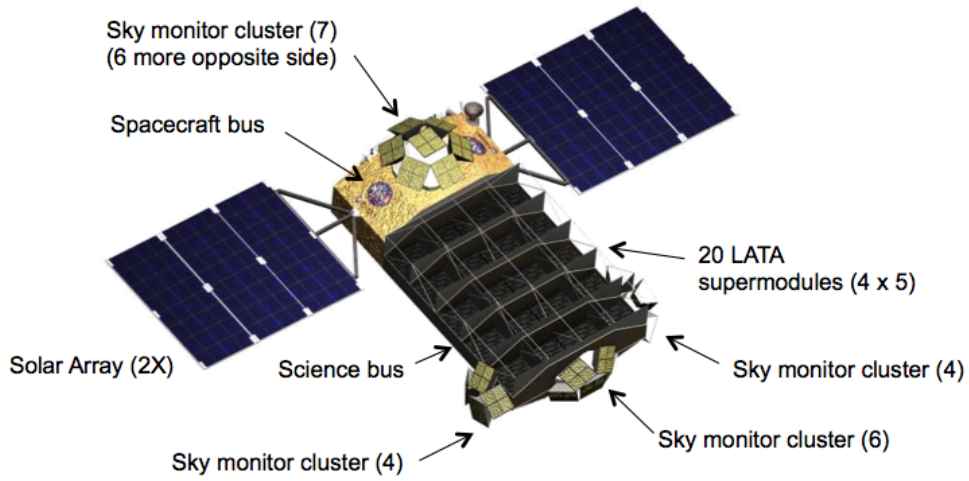


Figure 1. AXTAR spacecraft configuration with 20 LATA supermodules. This configuration is within the volume and payload mass limits for a Taurus II launcher, and will also easily work with a Falcon 9 launcher.

by RXTE to measure fundamental parameters of neutron stars and black holes and to study a broad range of topics in high-energy astrophysics. AXTAR was originally proposed as a medium-class probe concept in the 2007 NASA Astrophysics Strategic Mission Concept Study call. More recently, we have been developing AXTAR as a NASA Explorer-class mission concept. AXTAR's baseline main instrument, the Large Area Timing Array (LATA), is a collimated instrument employing thick Si pixel detectors that achieves 2–50 keV energy coverage and over 3 m² effective area. The mission also carries a sensitive Sky Monitor (SM) that acts as a trigger for pointed observations of X-ray transients in addition to providing high-duty-cycle monitoring of the X-ray sky. Several other large-area follow-on mission concepts have also been previously proposed.^{3–6}

We begin with a brief overview of the science objectives and mission drivers for AXTAR, then discuss our detector and mission concepts, and finally summarize the results of our recent mission design study.

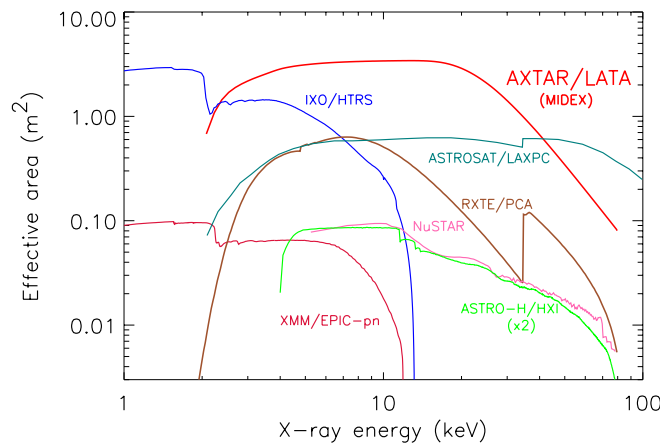


Figure 2. Effective area as a function of energy of the AXTAR LATA baseline detector concept. Several other current and planned missions are shown for comparison.

2. SCIENCE GOALS AND MISSION REQUIREMENTS

The natural time scales near stellar mass black holes (BHs) and neutron stars (NSs) (either the free-fall time or the fastest stable orbit time) are in the millisecond range. These time scales characterize the fundamental physical properties of compact objects: mass, radius, and angular momentum. For example, the maximum spin rate of a neutron star is set by the equation of state of the ultradense matter in its interior, a fundamental property of matter that still eludes us. Similarly, orbital periods at a given radius near a black hole are set by the black hole's mass, angular momentum, and the laws of relativistic gravity. Since its 1995 launch, RXTE has discovered millisecond oscillations from neutron stars that trace their spin rate and millisecond oscillations from accreting black holes with frequencies that scale inversely with black hole mass and are consistent with the orbital time scale of matter moving in the strongly curved spacetime near the black hole event horizon. However, while RXTE revealed the existence of these phenomena, it lacks the sensitivity to fully exploit them in determining the fundamental properties of neutron stars and black holes (see Ref. 2 and papers therein).

The large sensitivity gain of AXTAR's Large Area Timing Array will permit the exploration of multiple topics in the physics and astrophysics of compact objects, including:

- **Neutron star mass, radius, and equation of state.** AXTAR will extract information encoded in the pulse shapes of thermonuclear X-ray burst oscillations,^{7,8} kilohertz quasi-periodic oscillations^{9,10} (QPOs), and accreting millisecond X-ray pulsars^{11,12} to measure or constrain the fundamental properties of neutron stars. Asteroseismology of neutron star internal structure using X-ray oscillations during magnetar giant bursts will also be possible.^{13,14}
- **Black holes and the physics of strongly curved spacetime.** AXTAR will explore the physical origin of the stable, high-frequency QPOs observed in accreting black holes,¹⁵ testing their ties to black hole mass and spin. With its large effective area, broad energy coverage, and good energy resolution, AXTAR will also be an ideal instrument for time-resolved spectrophotometric study of relativistically broadened iron fluorescence lines in both black holes¹⁶ and neutron stars,¹⁷ as well as phase-resolved spectroscopy of low-frequency QPOs.
- **Physics of nuclear burning and exotic nucleosynthesis.** AXTAR will study thermonuclear X-ray bursts and superbursts from neutron stars with unprecedented sensitivity, allowing detailed time-resolution of burst rises, hot spot evolution, and the evolution of both early and late-time burst oscillations.¹⁸ AXTAR will be sensitive to spectral absorption edges from exotic heavy metals produced in the nuclear burning chains of radius-expansion bursts.¹⁹ AXTAR will also continue exploration of the mHz QPOs (interpreted as unstable nuclear burning on the neutron star surface) well beyond the limited instances accessible to RXTE.²⁰
- **Pushing the envelope.** AXTAR will provide clear detection or refutation of effects that were hinted at in RXTE data but remain unconfirmed. A leading example is provided by photon bubble oscillations,²¹ a radiation hydrodynamic effect predicted in accreting pulsars, but thus far detected with only marginal and disputed significance.²² If detected, these oscillations will probe the interaction of high intensity radiation with matter in accretion columns where the mass accreted per unit area far exceeds the Eddington limit.

The AXTAR Sky Monitor will monitor hundreds of X-ray sources in addition to serving as a trigger for target-of-opportunity observations of active X-ray transients. The activity level of Galactic X-ray sources is inherently variable on time scales from milliseconds to days to years. While RXTE demonstrated the need for a sky monitor as a trigger for pointed observations and to provide spectral and activity context about sources between pointed observations, we note that a sensitive sky monitor will serve as a primary science instrument for a wide variety of investigations, including:

- Daily monitoring of the flux and spin history of ~ 50 accretion-powered X-ray pulsars over 5 years, hence testing the theory of magnetic disk accretion and angular momentum transfer.²³ Dynamical measurement of orbital parameters through pulse timing for all of these systems.²³

Table 1. Mission Requirements

Parameter	Baseline	Drivers	Technology Factors
<i>Large Area Timing Array (LATA)</i>			
Effective Area	3.2 m ²	NS radius, BH QPOs	Mass, cost, power
Minimum Energy	1.8 keV	Source states, absorption meas., soft srcs	Detector electronics noise
Maximum Energy	>30 keV	BH QPOs, NS kHz QPOs, Cycl. lines	Silicon thickness
Deadtime	10%@10 Crab*	Bright sources, X-ray bursts	Digital elec. design, pixel size
Time Resolution	1 μ s	Resolve ms oscillations	Shaping time, GPS, Digital elec.
<i>Sky Monitor (SM)</i>			
Sensitivity (1 d)	< 5 mCrab*	Faint transients, multi-source monitoring	Camera size/weight/power
Sky Coverage	> 2 sr	TOO triggering, multi-source monitoring	# cameras vs. gimbaled designs
Source Location	1 arcmin	Transient followup	Pixel size, camera dimensions
<i>AXTAR Mission</i>			
Solar Avoidance Ang.	30°	Access to transients	Thermal/Power design
Telemetry Rate	1 Mbps	Bright sources	Ground stations/TDRSS costs
Slew Rate	> 6° min ⁻¹	Flexible scheduling, fast TOO response	Reaction wheels

*1 Crab = 3.2×10^{-8} erg cm⁻² s⁻¹ (2–30 keV)

- Phase-coherent tracking of the spin down of magnetars²⁴ using multi-day integrations and detection of rotational glitches,^{25,26} providing a window into neutron star interiors in the presence of superstrong magnetic fields. Detection of giant flares from magnetars in the Local Group.^{13,14}
- Long-term variability monitoring of the brightest active galactic nuclei (AGN) over hours, days, and years, testing how the variability timescale relates to black hole mass and this relationship extends to stellar-mass black holes.²⁷
- Identifying thermonuclear X-ray bursters entering a frequent bursting state. Detecting rare thermonuclear “superbursts” (deep nuclear burning events) as they occur, anywhere in the Galaxy. Statistical studies of thermonuclear burst activity over a wide range of mass accretion rates.^{18,28}
- Long-term timing of superorbital periodicities and accretion disk precession in low-mass X-ray binaries²⁹ (LMXBs). Orbital period evolution of eclipsing systems.³⁰
- Detection of gamma-ray bursts, X-ray flashes, and other short-timescale, isolated, or very low duty cycle flares.

In addition, the sky monitor offers partnership with observatories for wide-angle astronomy in other wavebands. New facilities are under construction for wide-angle radio monitoring such as LOFAR (30–240 MHz), the MWA (80–240 MHz), the LWA (10–88 MHz), and the Allen telescope (0.5–11 GHz). The correlated X-ray and radio exposures would radically change the landscape of investigations for the disk-jet connection for X-ray binaries and nearby active galactic nuclei.³¹ Partnerships would also be possible with new wide-angle optical monitors, e.g., the Large Synoptic Survey Telescope (LSST) and the Panoramic Survey Telescope and Rapid Response System (Pan-STARRS). Prime targets would include tidal disruption flares in nearby galaxies, a unique method to identify and measure the mass of supermassive black holes in non-active galaxies.

Furthermore, the Sky Monitor will also serve as the electromagnetic “eyes” for associated events that can be detected by gravitational wave observatories, such as Advanced LIGO and Advanced Virgo. As with all types of survey detectors, there is substantial value in processing data for a particular time and celestial position, compared to blind searches with so many more statistical chances to find enhanced noise. With its large field of view, the sky monitor could play a pivotal role to establish the reality of particular events, while helping to define the detailed science opportunities for gravitational wave detectors.

2.1 Mission Requirements

The requirements set by our science objectives are summarized in Table 1. We emphasize the following points:

- Our primary targets are bright Galactic X-ray sources. Since the sky background is negligible in this regime, there is no advantage in concentrating optics, and a simple collimated detector will suffice. In particular, the detector must be able to handle the high photon count rates from bright black-hole transients, thermonuclear X-ray bursts, etc., corresponding to fluxes as high as 10 Crab (3.2×10^{-7} erg cm $^{-2}$ s $^{-1}$, 2–30 keV), with minimal deadtime and pileup effects. Furthermore, the data system must be able to store and transmit these data at high time-resolution and adequate spectral resolution without losses. Finally, the detector must have large effective area at energies well above 10 keV in order to have good sensitivity to the millisecond phenomena identified by RXTE.
- Our required effective area is set by two key science objectives: (1) achieving a 5–10% neutron star radius measurement using pulse shape modeling and pulse phase spectroscopy of thermonuclear X-ray bursts, and (2) achieving 0.1% rms fractional amplitude detection threshold for high-frequency QPOs in accreting black holes. Note that, for QPO signals (i.e., resolved in frequency space), the signal-to-noise ratio of a given signal strength scales *linearly* with A_{eff} , rather than the usual $A_{\text{eff}}^{1/2}$ scaling.³²
- Our required lower energy bound is set by the need to determine temperature information from the thermal spectra of thermonuclear X-ray bursts, detect the soft thermal disk component of emission from accreting black holes, and measure interstellar photoelectric absorption toward our targets. Our upper energy bound is set by the need for sensitivity to high-frequency QPOs in black holes and kHz QPOs in neutron stars, both of which are hard X-ray phenomena with maximum amplitude in the 10–30 keV range.
- Many of our target observations need to be triggered to occur when the source is in a particular state; e.g., when an X-ray transient has emerged from quiescence into active outburst, or when an accreting neutron star is undergoing frequent thermonuclear X-ray bursts, or when an accreting black hole is in the particular spectral state where high-frequency oscillations are typically seen. This requires that the mission include a sky monitor capable of triggering observations. Since X-ray transients may appear anywhere in the sky at any time, and since there outbursts may be of short duration, this sky monitor should preferably cover the entire accessible sky (unocculted by the Earth and sufficiently separated from the Sun).
- RXTE has shown that the events that trigger target-of-opportunity (TOO) observations may be very short-lived. It is thus essential that the mission can be quickly rescheduled in a matter of hours, and that it can slew to new coordinates expeditiously.

3. DETECTOR CONCEPTS

For X-ray timing of bright sources, the key metric is effective area at the relevant energies with low deadtime, while background rejection and energy resolution are less critical than for some other measurements. Therefore, focusing or concentrating optics are generally best avoided in favor of large area detectors paired with collimators to limit the field of view and reject the diffuse X-ray background, which would otherwise be dominant.

Proportional counters have been the workhorse detectors for X-ray timing measurements since the early days of X-ray astronomy. The state of the art was moved forward by missions based on proportional counters like EXOSAT (1983–1986, $A_{\text{eff}} = 0.16$ m 2), Ginga (1987–1991, $A_{\text{eff}} = 0.4$ m 2), and most recently the RXTE (1995–2010, $A_{\text{eff}} = 0.6$ m 2). However, the use of proportional counters involves a number of challenges including modest energy resolution, significant dead times, large mass and volume per unit effective area, and a susceptibility to gas leaks and high-voltage breakdowns.

Recently, a significant developments in solid-state detector technologies have made possible a number of attractive replacements for massive gas detectors. A recent example is the Large Area Telescope (LAT) on NASA’s *Fermi* Gamma-ray Space Telescope, which has a tracker that contains ~ 75 m 2 of silicon strip detectors rather than the gas spark chambers used in previous experiments. The application specific integrated circuit (ASIC) readouts for the strip detectors were rather simple, requiring a fairly high energy threshold of ~ 30 keV and doing threshold event detection only, not spectroscopy.³³

In the case of AXTAR, however, a low energy threshold (~ 2 keV) and at least modest energy resolution are required. Since most solid-state detectors don’t internally amplify the signal, and a 2 keV X-ray liberates only

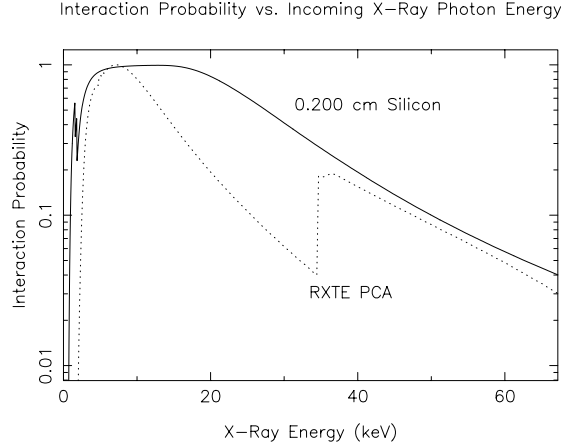


Figure 3. Comparison of the photoelectric interaction probability for an X-ray photon in 2 mm of silicon with that in the RXTE PCA xenon proportional counters. The efficiency improvement in the 15–30 keV energy range is evident and means that the sensitivity improvement in that range is much larger than just the increase in geometric area.

~550 electron-hole pairs in silicon, very low-noise pre-amplifiers are required to achieve these two goals. An important component of the noise budget in such a readout is proportional to the capacitance of the detector element and any interconnect to the amplifier. This motivates a search for low capacitance designs, and we briefly describe several alternatives here.

3.1 Baseline concept: Si PIN diodes

Our baseline design, described in more detail below, is to use large format (9×9 cm active area) thick silicon detectors that are divided into 2.5×2.5 mm pixels, each of which is effectively a simple PIN diode. At 2mm thickness, the stopping power of silicon in the critical 15–30 keV band is much higher than the 1 atm xenon proportional counters used in the RXTE PCA (see Figure 3). The pixels are connected to readout ASICs via either an interposer board that is bump bonded to the detector or by wire bonds through a grid of holes in the interposer board. This design is fairly straightforward and separates the design and fabrication of the ASICs from the detectors. One alternative is to adopt a hybrid detector design where the ASIC is identical in size and matched in pitch to the detector and the two are bump bonded together. An advantage of this design is that the interconnect capacitance can be made negligible compared to the pixel capacitance, potentially lowering the power requirement to achieve the required noise performance. The disadvantages of the hybrid detector approach may include low yields on very large ASICs and increased cost of fabrication for the large area ASICs.

3.2 Alternative concept: Si drift detectors and CdTe

An alternative is to replace the simple PIN diode pixels with a more advanced detector configuration, such as a silicon drift detector (SDD).³⁴ An SDD uses carefully shaped electric fields to direct the charge from a relatively large pixel to a very small collecting anode, thus greatly reducing the effective capacitance of the pixel. This results in significantly improved energy resolution with reduced power requirements. However, SDDs are a newer technology and are just now starting to be made in large area formats. Moreover, they have thus far been limited to fairly thin detectors (~0.5 mm), so they may not have sufficient sensitivity above 10 keV for our science requirements. One way to address that limitation would be a hybrid design, with most of the area devoted to SDDs but a portion instrumented with cadmium telluride (CdTe)³⁵ or another technology with good high-energy sensitivity. An advantage of this hybrid approach is improved spectral fidelity at high energies relative to the thick-silicon option. At 30 keV, Compton scattering (and incomplete energy deposition) accounts for more than 10% of incident photon interactions in silicon but is a negligible effect in CdTe. (Note that the xenon gas detectors in earlier missions also had negligible Compton scattering at these energies.)

All of these designs share several advantages of low dead time due to the independent readout of each pixel and can provide precise timing, energy, and pixel coordinates for each detected X-ray photon. For our current

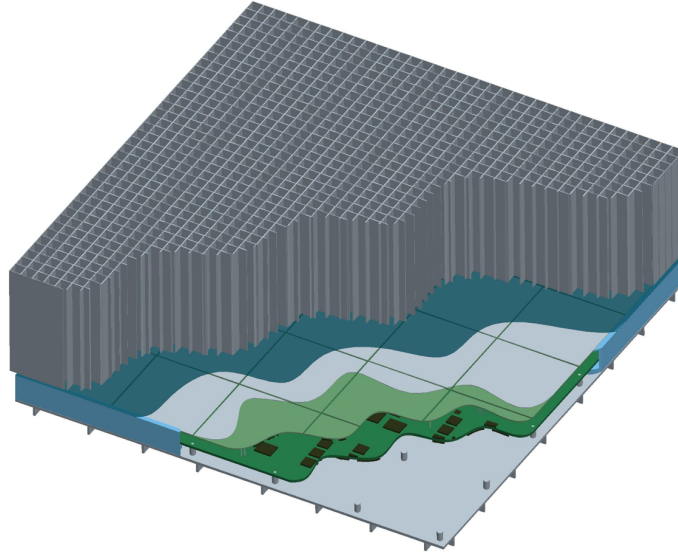


Figure 4. Cutaway rendering of a LATA supermodule consisting of a 5×5 array of 10×10 cm detectors. The components from top to bottom are the collimator, light shield, silicon detectors, interposer board, and digital board, mounted in a box that provides support and shielding. Note that the collimator cell size is not to scale.

concept study we have used the simple silicon pixel design as a baseline. We will continue to study the alternatives and if one is mature enough to be preferred, it will be substituted into the design. From a mission design point of view this substitution will mainly reduce the power requirement and improve the energy resolution of the detectors.

4. SCIENCE INSTRUMENTS

4.1 Large Area Timing Array (LATA)

The primary instrument on AXTAR is the Large Area Timing Array (LATA). For the LATA, we have chosen a modular design, consisting of an array of identical, but independent, detector ‘supermodules’, each of which consists of a detector plane mated to a collimator and including support electronics (see Figure 4). This modular design ensures easy scalability to different size missions, robustness to individual failures, and simplifies assembly and testing.

Each supermodule consists of a 5×5 array of detectors, front end electronics, a digital interface to the Instrument Data System (IDS), and low and high voltage power supplies. The baseline detectors (see Figure 5) are manufactured using 150 mm diameter high-resistivity wafers that are 2.0 mm thick. The detectors are $96 \text{ mm} \times 96 \text{ mm}$ in size with an active area of $90 \text{ mm} \times 90 \text{ mm}$ and with a 3 mm wide guard structure around the perimeter of the detector. Each detector is segmented into a two-dimensional array of 36×36 pixels, each with an area of $2.5 \times 2.5 \text{ mm}^2$. This segmentation was selected to minimize the noise of the analog read-out electronics for a given power budget, in this case 1 W per detector. A single contact that is biased at high voltage ($\sim 700\text{V}$ for this thickness) covers one side of each detector; this is the side exposed to the incoming X-radiation. Each supermodule thus provides 2025 cm^2 of total active area, which becomes 1720 cm^2 of active area for a collimator open fraction of 0.85.

In the baseline design, the silicon detectors are bump bonded to an interposer board that provides mechanical support and connections to the critical front-end electronics. The interposer board is manufactured from very low dielectric loss material and the traces are designed to minimize stray capacitance from the connection. To keep the trace lengths low, the readout ASICs have 36 input channels and read out a 6×6 array of pixels. A

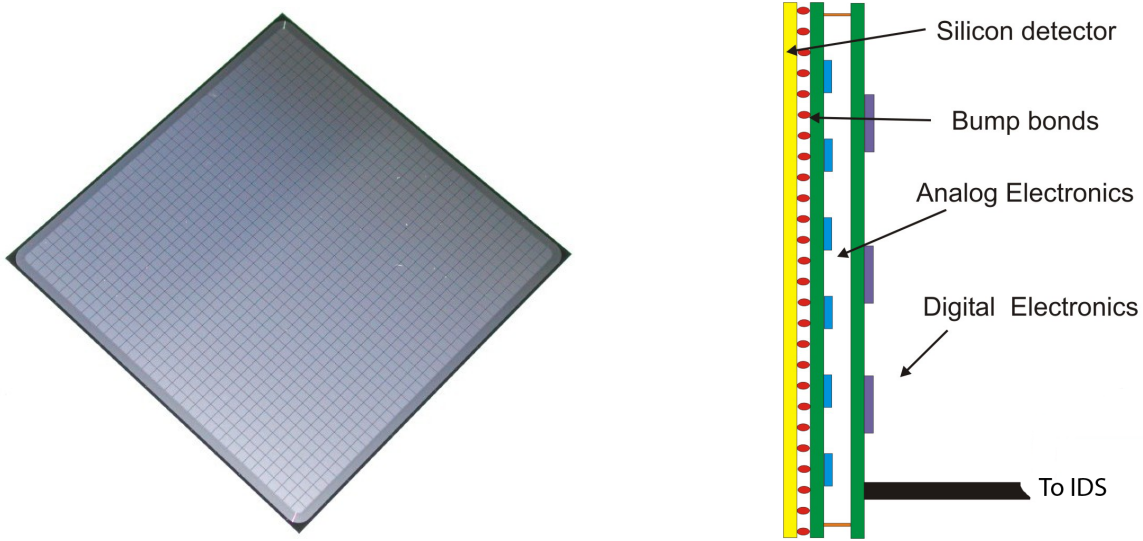


Figure 5. **Left:** Photograph of a pixelated silicon detector for both the LATA and SM instruments with 36×36 pixels covering a total active area of $90 \text{ mm} \times 90 \text{ mm}$. **Right:** Side view of a LATA/SM detector assembly showing the layered construction of the detector module.

total of 36 ASICs are required to read out all 1296 pixels on the detector. Preliminary modeling shows that using Rogers 5870/5880 material (with a dielectric constant of 2.4/2.33), the capacitance per pixel will be between 0.3 pF and 0.6 pF, depending on the pixel position. If more than 36 pixels are connected to a single ASIC, the loss of performance due to the capacitance from the traces outweighs the power savings and the overall performance is degraded.

The critical readout ASIC must be designed to be both low power and low noise to achieve the required low energy threshold of 2 keV. To achieve an acceptable limit on noise-induced counts in the electronics, we compute that the equivalent noise charge (ENC) of the amplifier must be < 77 electrons r.m.s. We thus set the design goal for the front end ASIC at 70 electrons r.m.s. to provide some margin. With this noise, the detector will have an energy resolution of 600 eV FWHM. This energy resolution would be nearly constant over the full energy range of the detector. The BNL group has designed a similar ASIC³⁶ that meets the AXSTAR performance goals by more than a factor of two, achieving an energy resolution of 173 eV at 6 keV, but consumes a factor of two more power (1.6 mW/channel) than our budget. Development of a new CMOS ASIC design with lower power is planned. The functions performed by the ASIC include charge amplification, shaping, threshold discrimination, peak detection, and multiplexing of the output to the digital board. The ASIC will also include circuitry to adjust gain settings, inject calibration pulses, mask off bad channels, and set discriminator threshold levels.

All the digital electronics for a module will be located on a second board with the same form factor as the detector and interposer board. This board will contain the analog-to-digital converter (ADC) and a Field Programmable Gate Array (FPGA). The FPGA will control the detector ASICs and the ADCs. The digital electronics board will produce a stream of time-tagged events that will be sent to the Instrument Data System (see §4.3).

Our baseline collimator concept is based on the design used for the RXTE PCA.³⁷ There will be one $50 \times 50 \times 20 \text{ cm}^3$ collimator per supermodule, with a nominal field of view of 1° (FWHM). Each collimator module is manufactured from Be-Cu foils. Each collimator will support a thin film thermal shield that is largely transparent at $E > 2 \text{ keV}$ to the incoming X-radiation. Because of the small mass of the silicon detectors, the mass budget of the instrument is dominated by the collimators. We are continuing to study alternative collimator designs that could reduce the instrument mass without significantly degrading the performance. In addition to the collimator, there will be a graded-Z (e.g. Ta-Sn-Al or Ta-Cu-Al similar to what was used for the RXTE PCA³⁷ and the Swift BAT³⁸) shield on the back and sides of the instrument, primarily to block diffuse cosmic X-rays from hitting

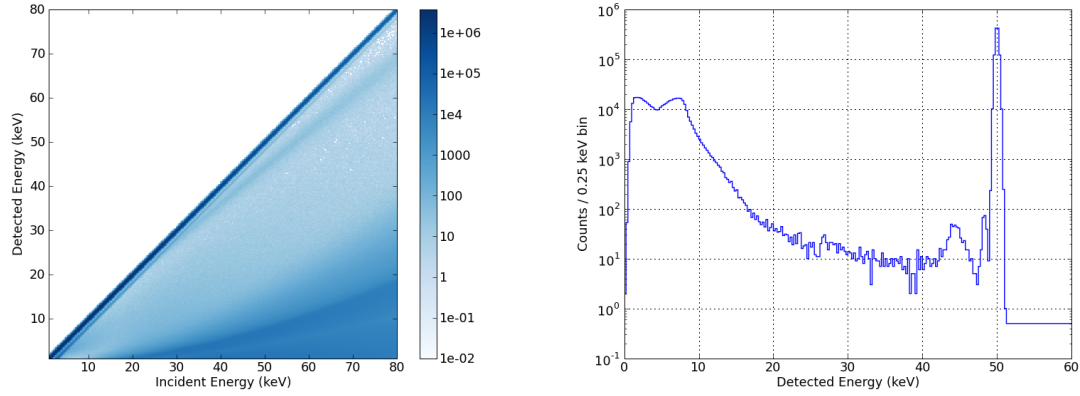


Figure 6. Response matrix simulation results for a baseline 2-mm thick LATA silicon detector. The panel at left shows the 2-dimensional response matrix with detected energy as a function of incident photon energy, with a log color scale. The effects of escape of fluorescence photons and Compton scattering are responsible for the non-diagonal terms. At right is the response for monochromatic 50 keV incident photons.

the detector. Because the Sun becomes an exceedingly bright source of soft X-rays during solar flares, we also include sun shields (nominally 0.2 mm thick lead foils) that keep the Sun from directly illuminating the front of the collimators for all pointing directions $> 45^\circ$ from the Sun. This prevents singly-scattered solar X-rays from being a significant background source during periods of high solar activity.

Each complete supermodule has an estimated mass of 30 kg and a power budget of 30 W. For the electronics to maintain their noise performance, they must be maintained at a temperature of 10°C or lower.

We have modeled the AXTAR LATA spectral response using the **Geant4** particle simulation program.³⁹ In these simulations we illuminated one LATA module of 9 cm by 9 cm silicon (2 mm thick) with a monochromatic beams of 10^7 X-ray photons oriented normal to the detector face spaced at 0.25 keV intervals covering the range 1.25 to 80 keV. The simulations include a detailed treatment of many radiative effects including photoelectric absorption, fluorescence, and Compton scattering of the injected photons. Our primary interest here is to understand the effects of Compton scattering on the spectral response of the LATA. Figure 6 shows the simulated response of the LATA module. The left panel is a summary of the resulting detected energies from illuminating the silicon. Photoelectric absorption of X-rays leads to the primary photopeak and associated escape peak at the energy of the injected photons. However, Compton scattering results in a continuum of detected photon energies at lower energies within the LATA energy range. The detailed redistribution of 50 keV photons by the active silicon is shown in the right hand panel. The spectrum of detection energies from each discrete injection energy can be utilized to create an energy redistribution matrix for each input X-ray energy. This redistribution function is then incorporated into a response matrix suitable for simulation of the LATA response to astrophysical source spectra.

The instrument must reject several types of backgrounds, most importantly from charged particles in the space environment. Low energy charged particles will be stopped by the same shielding that blocks diffuse X-rays but shielding against high energy particles can never be completely effective. The passage of high-energy charged particles through the detector will almost always produce ionization that is equivalent to a photon of energy of > 50 keV or more; i.e., well above the sensitive band of the instrument, and can therefore be rejected by an energy cut on the detected signal. Particles that “nick a corner” of a pixel will need to be identified on the basis of a coincidence with a high energy event in a neighboring pixel. In any case, there are a number of means of identifying and rejecting all types of non-X-ray-induced events with efficiencies that should be adequate.

4.2 Sky Monitor (SM)

The AXTAR-SM is designed to independently pursue the science themes of wide-angle X-ray astronomy (§2), which includes the detection of target opportunities for AXTAR pointed observations. However, the SM will

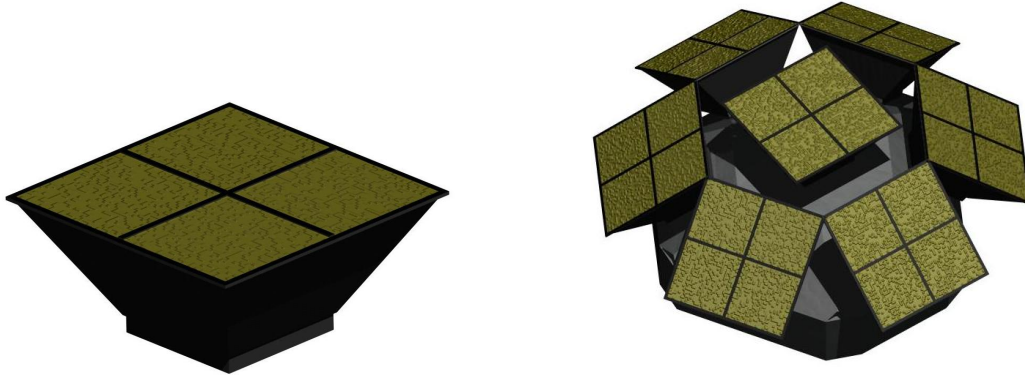


Figure 7. **Left:** Rendering of a Sky Monitor camera. **Right:** A cluster of 7 SM cameras.

not drive a major increase in the overall cost of the mission, as it is constrained to require no more than $\sim 20\%$ of the resources required for the LATA, i.e., for cost, mass, volume, downlink rate, and power. The design is greatly facilitated by using precisely the same detector technology developed for the main detector array and by avoiding the use of moving parts. The SM operations plan should not impose any constraints on the LATA observing program. Furthermore, the SM cameras must be able to be pointed anywhere in the sky, including fields containing the Sun, although no useful data will be produced from a camera while the Sun is in its field of view.

The baseline design for the SM is a set of coded-mask cameras with detector planes consisting of a 2×2 array (300 cm^2 total effective area) of the same Si pixel detectors (2.5 mm pitch) used for the LATA. Each 2×2 detector array will be mounted in a camera body topped with a 2-D coded aperture mask (see Figure 7). Each camera will be approximately 25 cm square at the base (detector end) and 30 cm square at the aperture plane. The total height will be approximately 45 cm. The cameras are relatively light; each will have a mass of a few kilograms, at most.

The field of view of each camera will be approximately $40^\circ \times 40^\circ$ (FWHM) or about 0.4 sr. For this size field, full sky coverage requires a complement of 32 cameras. The concept that was studied in detail in the recent exercise comprised 27 cameras, grouped in 5 clusters. This instrument would achieve $\sim 85\%$ all-sky coverage (to FWHM), with most of that coverage having uniform effective area. Further coverage losses are expected from Earth occultation (33%), passages through the South Atlantic Anomaly (an additional 7.5% at 28° orbit inclination, and 2% at 5°), and AXTAR slews (few %). In the end, the AXTAR-SM can achieve an average of 50–55% in all-sky live-time coverage, which far exceeds the levels of previous missions (see §2).

Thus far, the best wide-angle X-ray monitors have achieved duty cycles per source: $\tau = 0.020 \pm 0.005$, depending on ecliptic latitude, for the RXTE All Sky Monitor (ASM), and $\tau = 0.010$ for the Beppo-SAX Wide Field Camera (WFC). For bright X-ray transients, RXTE pointed observations are typically conducted with $\tau = 0.025$, while a singular large-program experiment for the 2005 outburst of GRO J1655-40, achieved $\tau = 0.096$. These values are insufficient to capture critical, infrequent events that convey the greatest leverage for constructing detailed physical models. The Swift BAT (1.4 sr FOV) is producing hard X-ray light curves (15–50 keV) for XRBs with $\tau \sim 0.10$. These data are extremely useful in many ways, but for the investigations of accretion disks, state transitions, and the disk:jet connection, there is the limitation that the BAT sensitivity is above the spectral range of both black hole and neutron star disks (typically 0.5–1.5 keV at the inner boundary) and also the neutron star boundary layer (blackbody $T < 2.7 \text{ keV}$).

In the current AXTAR design, the capability of the SM to achieve $\tau = 0.5$ is a historical step forward, as illustrated in Figure 8. This provides data at the times critical interest for diverse science topics outlined in §2. Furthermore, the one-day sensitivity would be improved by almost an order of magnitude, compared to the RXTE ASM, reaching 1 mCrab at 4σ , or $1 \times 10^{35} \text{ erg s}^{-1}$ at the Galactic center. An archive of good events

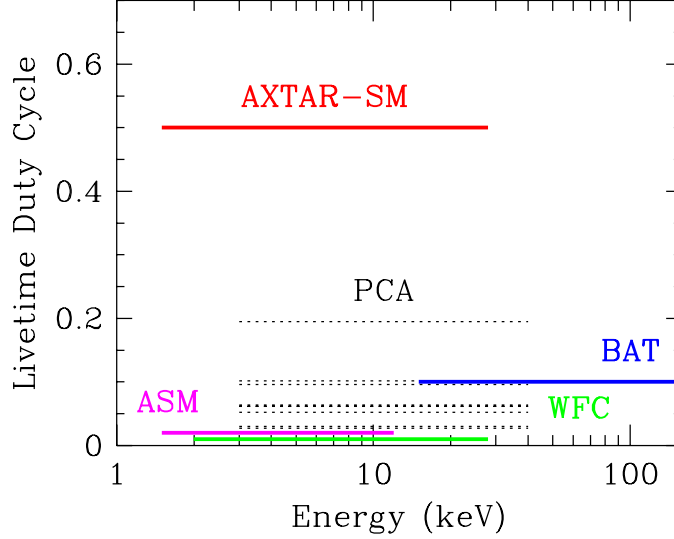


Figure 8. The livetime duty cycle of various X-ray instruments plotted versus photon energy. Solid, colored lines show all-sky livetime averages (τ) from wide-angle X-ray monitors. The dotted lines show the highest duty cycles achieved for individual sources during monitoring campaigns of several days with the RXTE PCA instrument. The AXTAR-SM, in the 27 camera case, can achieve $\tau = 0.5$, or higher, while its bandwidth (2–30 keV) is sensitive to both the thermal and non-thermal components radiated by accreting black holes and neutron stars.

from the SM with excellent time resolution (e.g., 122 μ s) would provide retrospective capability to process data for any position, at any time of interest.

4.3 Instrument Data System (IDS)

The LATA will generate 120 kcts s^{-1} from the Crab, 0.5 Mcts s^{-1} from a 4 Crab black hole transient, and 1.2 Mcts s^{-1} from Sco X-1! An event-by-event mode with, e.g., 40 bits per event would require a 5 Mbps data stream during observations of a 1 Crab source. Therefore adequate data handling capability is crucial to maintain event throughput and to optimize the usefulness of the data products that are chosen for transmission within the limit of telemetry bandwidth.

RXTE had great success observing bright sources by using a highly flexible Experiment Data System (EDS) with programmable data modes that could maximally utilize the telemetry bandwidth available. We propose a similar data system for AXTAR, the Instrument Data System (IDS). The IDS will, like the the EDS, generate multiple data products for the LATA by using event handlers, in parallel, to implement each chosen data “mode”. This will allow, e.g., capture of one data stream with the full energy resolution of the detectors at low time resolution, while also sending down data at very high time resolution with modest energy resolution in another stream. If the number of counts per time or energy bin is much greater than unity (as it would be for bright sources or low time resolution), the data will be binned. If it is much less than unity, then the telemetry would be minimized by transmitting the elemental data for each photon event. The IDS will be fully reprogrammable to allow it to adapt to new ideas, new discoveries, and other unexpected conditions. On the other hand, we expect that one or two “standard modes” will always be operating to create a uniform data set to facilitate archival analyses.

5. MISSION DESIGN

In this section, we describe the baseline mission design, developed as part of a mission concept study at the MSFC Advanced Concepts Office. RXTE, launched in 1995, cost more than \$200M. In our evaluation, it is not feasible to build a successor mission with a factor of several more geometric and effective area within the confines of a NASA SMEX (the last call was in 2008 for \$105M, not including launch) or EX class mission (anticipated

Table 2. AXTAR mission study parameters

Parameter	Required Value (Desired or Maximum Value)
AXTAR spacecraft	
Orbit Altitude	~ 600 km (study output), circular
Orbit Inclination	28.5° or less (as low as possible)
Spacecraft Lifetime	3 yr
Consumables	> 5 y
Orbit Lifetime	10–15 yr
Pointing Accuracy	< 1 arcminute
Pointing Knowledge	< 5 arcsec
Maximum Slew Rate	180 deg in 30 minutes
Maximum Continuous Observing Time	28 hr
AXTAR Sky Monitor camera (each)	
Mass	2 kg + 2 kg per telemetry hub
Power	4W + 9W per telemetry hub
Quantity	7 minimum (32 maximum)
Thermal requirement	-40°C to $+10^\circ\text{C}$ (detector plane)
Alignment	32 faces and vertices of dodecahedron
AXTAR LATA supermodule (each)	
Mass	30 kg
Power	30W
Quantity	20 (as many as possible)
Thermal requirement	-40°C to $+10^\circ\text{C}$ (detector plane)
Alignment	all co-aligned within 1 arcminute
Contingency Philosophy	
Mass	30% for spacecraft subsystems and instruments
Power	30% for spacecraft subsystems and instruments

2010 for \$200M, not including launch). However, with the cost and mass savings possible using large area solid state detectors, we believe that a major improvement over RXTE can be made with a MIDEX class mission. For planning purposes, we hypothesize a 2014 call for proposals for a \sim \$300M (not including launch) class mission to be launched in 2019.

5.1 Assumptions and Requirements

The spacecraft was designed to meet the requirements listed in Table 2. As the requirements are relatively modest, no new technologies are needed for the spacecraft to enable the science mission. The Table also include key data on the science instruments that affect mission design.

5.2 Mission Analysis

The orbit selection was driven primarily by three criteria: to minimize passage through the South Atlantic Anomaly (SAA), to avoid radiation at the higher altitudes, and to avoid as much atmospheric drag as possible. While lower inclinations help with avoiding the SAA, the science instruments can be turned off during these periods, so this is not a driving requirement. In order to avoid higher radiation exposures, the altitude must be limited to not much more than 600km. And finally, avoiding atmospheric drag requires a higher altitude orbit, preferably one in which natural orbital decay will not result in re-entry sooner than 10 years after orbit insertion, which minimizes station-keeping. Using the NASA Debris Assessment Software (DAS 2.0)⁴⁰ and Analytical Graphics Satellite Tool Kit (STK)*, the team determined through parametric analysis that the optimal initial orbit would be a 585 km circular orbit, with the goal for the launch vehicle to insert the observatory into as low of an inclination as possible. To be slightly conservative, the initial orbit altitude for use in determining launch vehicle performance was set to 600 km.

*<http://www.agi.com>

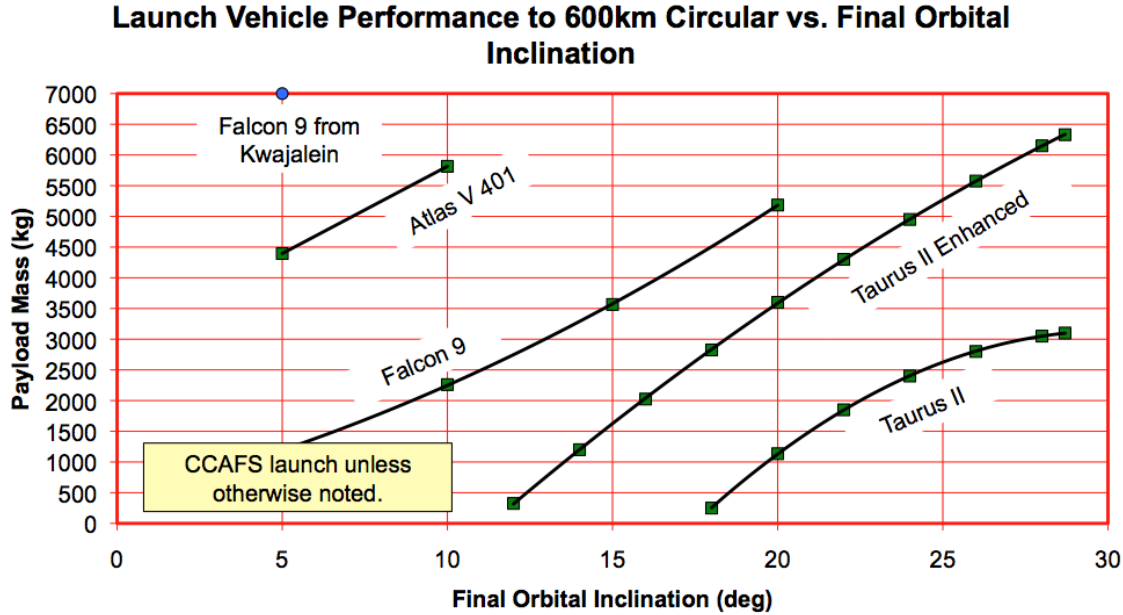


Figure 9. Payload mass versus inclination for various launch vehicles.

Using historical spacecraft data for other science missions, the team estimated the observatory mass would be approximately 2000kg for a configuration with 20 LATA supermodules. Given this mass, and the estimated area required by 20 LATA supermodules, the team chose two launch vehicle candidates: the Orbital Sciences Corporation's Taurus II, and the SpaceX Falcon 9 (which had a successful inaugural flight on June 4, 2010). Since both vehicles can use the same payload adapter, a spacecraft that will fit within the Taurus II shroud will also fit within the Falcon 9 shroud, giving at least two vehicle options for the spacecraft. Performance estimates for the Taurus II came directly from Orbital Sciences Corporation;⁴¹ for the Falcon 9, the data were provided by NASA Launch Services Program[†]. Since the goal is to achieve as low an inclination as possible, any excess payload capability provided by the launch vehicle will be used to lower the orbital inclination. The payload maximum mass versus inclination for various launch vehicles is plotted in Figure 9. Note that launching the Falcon 9 from Kwajalein results in the most mass to the lowest inclination, but may incur additional costs. The Taurus II Enhanced data are very preliminary, as this vehicle is still in the design phase, and is offered only for comparison.

5.3 Spacecraft Configuration for Taurus II Class Launch Vehicle

The driving factor in the spacecraft's configuration was the launch vehicle size which limited the number of primary science instruments (LATAs). The LATAs coplanar and pointing requirements drove the design layout to be divided into two main sections, a spacecraft system bus and a science bus. The science bus/LATA array was set forward to provide separation from the spacecraft's solar arrays and other systems. The spacecraft system bus is located aft near the launch vehicle interface to carry launch vehicle loads and to allow for the spacecraft's systems to be enclosed in a more compact volume.

The other design factor was the number and placement of the sky monitor cameras. A configuration using the 32 combined faces and vertices of a dodecahedron would allow full sky coverage but due to volume and operational constraints 27 were chosen for the baseline configuration. These were broken up into several clusters and placed on the spacecraft to optimize viewing angles while minimizing size. The overall configuration is conservative and does allow room for component growth and for extra subsystem components to be added that were not analyzed in this study. The design has continuous load paths and structures which allows for minimum

[†]<http://elvperf.ksc.nasa.gov/elvMap/>

Table 3. Master equipment list and mass budget (Taurus II configuration)

Equipment	Mass (kg)
Structures (incl. LATA radiation shielding)	745
Propulsion	66
Power	137
Avionics, Control, Comm	189
Thermal Control	39
Contingency (30%)	351
DRY MASS	1527
Non-propellant fluids	4
LATA (20) supermodules	600
Sky Monitors (27)	54
Instrument Data System	20
Payload contingency (30%)	202
Instrument cabling	35
INERT MASS	915
TOTAL LESS PROPELLANT	2442
Propellant (Hydrazine)	208
GROSS MASS	2650

mass to be obtained. The design, while based on the Taurus II launch vehicle, could be used on comparable (not smaller) size launch vehicles. If a larger launch vehicle was selected a different overall configuration and layout would need to be studied to achieve the optimal configuration.

The design includes a 30% mass and power contingency for all spacecraft systems and for all science instruments. The spacecraft design for the Taurus II resulted in a total vehicle gross mass of 2,650 kg, which is outlined in the table below. Gross mass is the combined total of vehicle dry mass, inert mass, and propellant. Dry mass is defined as spacecraft subsystems mass minus the useable propellant, propellant residuals, and science instruments. Inert mass includes propellant residuals and science instruments.

5.3.1 Spacecraft Structure

The octagonal AXTAR bus provides a launch vehicle adapter and structure to mount all instruments and 27 sky monitors providing nearly full sky coverage, as well as, maintaining 20 LATA supermodules in a coplanar array. Radiation shielding against cosmic and solar radiation is incorporated into the spacecraft bus, and is considered as part of the spacecraft structural mass in Table 3. The spacecraft utilizes lightweight 2024-T351 aluminum panels, tubing struts, and frames for component mounting and to double as radiators for thermal management. Two flight-proven telescoping solar array booms⁴² are stowed against the spacecraft bus for launch. A load set of combined Taurus II/Falcon 9 loads, 6.0 g axial and 2 g lateral, was applied at 30 and 45 degrees around the launch axis. Finite Element Modeling Analysis and Post-processing (FEMAP) verified a positive Margin of Safety for a spacecraft structure loaded with instrument masses and analyzed with NX NASTRAN using a 1.4 Factor of Safety for isotopic strength.

5.3.2 Communications System

At present, the downlink data rates for this mission are within the capabilities of a system using a fixed antenna. A communication link to ground using fixed antennas is desirable over an active pointing design because it eliminates gimbaled mechanisms, and using an omni-directional antenna is more reliable and reduces mission risk. Analysis shows that using an X-band system with omni antennas for the science data downlink is sufficient for the given data rates and assumed mission scenarios. Using TDRSS for normal operations and data link is an alternative design that was not pursued in this study. However, a TDRSS link during launch and start-up operations is desirable. The communication system designs are single fault tolerant.

For this mission, low orbit inclinations are better for science data collection. A ground link analysis based on link times and daily accesses was performed to determine the best selection of ground stations at both 5 and 28 degrees. Out of eleven possible ground stations analyzed, Southpoint Hawaii and Kourou Guiana were selected as the primary and secondary ground link stations respectively for 28 degree orbits. These same two stations are also selected at a 5 degree orbit, where Kourou becomes the primary and Southpoint becomes the secondary stations.

At these two stations, at least an 8 minute primary link is possible 7 times a day. Under a worst case condition, a 6.7 minute link 5 times a day is possible for the 5 degree inclination at the secondary Southpoint station. Using these two conditions as bounds, a link budget was performed assuming at least 4 links per day for 8 minutes each. For these link times, it was found that a 20 watt transmitter can achieve a 90 Mbps data downlink rate. At this rate, almost 44 Gbits can be transmitted per station pass, or 172 Gbits per day. Assuming a continuous average data rate of 700 kbps for the entire LATA system and 72 kbps for an 8 unit SM cluster, enough link capability is left to download over six 15 minute peak (19 Mbps) LATA events per day. Major SM events can be alternated with LATA event data, assuming the SM detects events first and then the LATA is pointed to the event. The suggested 20 watt L3 X-band transmitter is presently at TRL[‡] 6.

An estimate for the total spacecraft telemetry communication data rate using S-band is 60 kbps downlink and 4kbps uplink. Using a 5 watt S-band transmitter, a link to TDRSS for launch and start up operations can be accomplished at these data rates, again using omni antennas. The 5 watt transmitter can also easily link with ground for normal telemetry with plenty of margin available. The suggested AeroAstro 5 watt S-band transmitter is at TRL 8.

5.3.3 Power Systems

The overall power demand, including the spacecraft, science instrumentation and 30 percent growth margin, is 1583W for the Taurus II configuration. The Power System supplies all of this demand. Power is generated by conventional, rigid panel solar arrays configured from space-qualified GaAs 3-Junction cells. The solar array regulation, power conversion, and power distribution is performed by a set of VME power electronics boards designed for use on the Mars Reconnaissance Orbiter and Orion spacecraft. All power function circuits are redundant and the boards are hosted in a single VME enclosure with redundant power supplies. The bus voltage is 28V. Energy storage is provided by Lithium Ion batteries configured from existing, space qualified cells. The maximum depth of discharge allowed is 40 percent. One 'Hot Spare' battery is carried for redundancy. The power system mass (including 30 percent contingency) is 179 kg for the Taurus II configuration.

5.3.4 Avionics and GN&C

Two fully redundant Proton 200 flight computers from SpaceMicro are the core of the avionics system. The computers are used for spacecraft operations and data management. They receive processed science data from the IDS, and transfer the data to either the on board data recorders or the X-band transmitters for downloading. Two data recorders from Surry Satellite Technology can store up to 256 Gbits of data at a rate of 150Mbps. One day of required data storage is estimated to be about 173 Gbits, giving approximately a 50% memory margin. The flight computers are radiation hardened to 100 krad total ionizing dose and 70 MeV-cm²/mg single event latch-up. The Proton 200 is scheduled for its first launch in 2010, and is presently at TRL 6. The Surrey data recorders are at TRL 8.

Attitude knowledge is achieved using a redundant pair of Ball Aerospace star trackers and Northrop Grumman IMUs. The star trackers provide 4 arcseconds of accuracy, meeting the 5 arcsecond mission requirement. Both the IMUs and the star trackers are at or above TRL 8.

While this satellite has large surface areas resulting in significant disturbance torques, the slewing and pointing requirements are modest. Off-the-shelf reaction wheels should be sufficient for attitude control, keeping cost down. In low earth orbit, magnetic torque rods are good candidates for attitude control assistance and reaction wheel desaturation. Using magnetic torquers, the spacecraft reaction control system will not normally be required for

[‡]Technology Readiness Level, see http://esto.nasa.gov/files/TRL_definitions.pdf

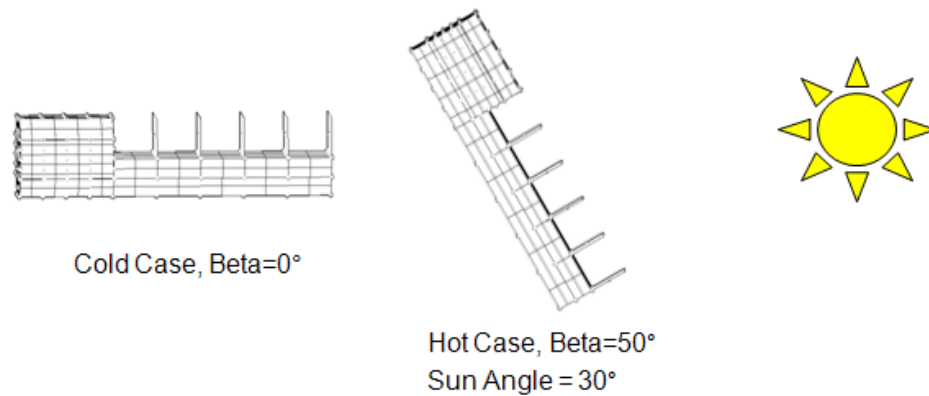


Figure 10. Spacecraft orientations used for the hot and cold thermal cases.

attitude control, and is considered for contingency purposes and disposal only. A set of 3 dual coil Microcosm MT400-2 magnetic torquers is suggested for this mission. These torquers are at or above TRL 8.

The trade space for reaction wheels included 4 different wheel types at four slewing speeds. This trade resulted in a Teldix RSI 68-170 reaction wheel being selected. Mounted in a 4 wheel pyramid configuration for best performance while maintaining one fault tolerance, these wheels have sufficient momentum and torque capability to exceed the fast slew requirement of 180 degrees in 30 minutes, while providing the desired pointing accuracy of 1 arcminute. The Teldix wheels are at or above TRL 8.

Inertial pointing will be the typical pointing mode for science observations. In this mode, the magnetic torque rods provide good torque authority. Using the torquers to offset the disturbances, the 28 hour continuous pointing goal can be achieved, with unlimited pointing times possible. In a zenith pointing mode, a possible scanning mode, the disturbances will usually be small. In this pointing mode desaturation of the reaction wheels can be accomplished using the magnetic torque rods. In a worst case torque scenario the atmospheric and gravity torques are at a continuous maximum. If left in this mode for extended periods the reaction wheels will eventually saturate. However, extended pointing times in this mode are unlikely since there are no apparent science advantages. If wheel saturation does ever occur, a return to zenith pointing for quick desaturation is possible.

5.3.5 Thermal Control System

Thermal control of the AXTAR spacecraft will utilize passive components including multilayer insulation, high emissivity paint and coatings, heaters, etc. to maintain spacecraft subsystem components within acceptable temperature ranges.

A system level thermal model was developed in Thermal Desktop[§]. The structure is modeled as aluminum and the panel thickness is consistent with the structural design. Structural panels double as radiative surfaces. Environmental heat loads were calculated for an earth orbit altitude of 585 km. Spacecraft structure temperatures for both a hot and cold orientation were generated. The hot orientation is defined as a LATA-to-sun angle of 30 degrees with a beta angle of 50 degrees; the cold orientation is defined as a LATA-to-sun angle of 90 degrees with a beta angle of 0 degrees (see Figure 10).

Subsystems equipment and experiment heat loads are imposed directly on the structure and modeled as area averaged heat loads. RCS thrusters, antennas, solar arrays and array mechanisms are not part of this preliminary analysis, nor is experiment temperature prediction included. The analysis predicts that all interface temperatures are within an acceptable range. The estimated total mass for the thermal control system is 50 kg, which includes a 30 percent margin.

[§]C&R Technologies, Littleton, CO, <http://www.crtech.com>

5.3.6 Propulsion System

The propulsion system's primary function is to de-orbit the spacecraft at the end of the mission and to provide attitude control during each maneuver. A simple monopropellant blowdown system, with maximum use of off-the-shelf components, is selected for this task. The system consists of three ATK 80488-1 diaphragm tanks that are loaded with hydrazine propellant and nitrogen pressurant. The thruster configuration includes four pods, each containing one Aerojet MR-104A/C (100 lbf) engine and two MR-106L (5 lbf) engines; two of the four larger thrusters are designated as backup. This engine thrust combination is selected to maintain low gravity-losses during the de-orbit burns, allowing the use of the above-stated tanks. All the tanks are loaded to capacity with 210.0 kg of hydrazine and 2.4 kg of nitrogen. The basic dry mass of the entire system is 66 kg. Adding 30% for growth raises the dry mass to 85 kg. The resulting total wet mass of the propulsion system is 298 kg.

6. CONCLUSION

RXTE is approaching the end of its mission life, concluding a mission that has brought enormous returns in every area of X-ray timing science. A successor mission needs to make a major advance by bringing observing capabilities beyond those of RXTE. Only a mission with timing as its central objective will address the science goals described in Section 2. The central technical challenge is to achieve collecting area many times larger than RXTE, extending the observed band to higher X-ray energy, and with mission architecture to identify targets (using a sky monitor), execute optimized pointing sequences, and to handle the high data rates on bright sources, all at affordable cost. AXTAR is mission concept that will do all these things; this paper has reported the first thorough study of what is involved in producing such a mission. It will reach the driving goals of constraining the neutron star equation of state and using plasma motions in curved space near black holes to probe black hole physics. The same facility will support a diverse range of other investigations similar to those that made RXTE successful, but superseding RXTE by reaching lower levels of modulation, shorter timescales and higher temporal frequencies.

ACKNOWLEDGMENTS

This work was supported in part by the NRL 6.1 Base Program funding; NASA APRA program NNG10WF45I; the MIT Kavli Instrumentation and Technology Development Fund; and the Technology Investment Program at NASA Marshall Space Flight Center.

REFERENCES

- [1] Lamb, F. K., "Scientific Challenges for a New X-ray Timing Mission," in [*X-ray Timing 2003: Rossi and Beyond*], Kaaret, P., Lamb, F. K., and Swank, J. H., eds., *AIP Conf. Ser.* **714**, 3 (2004).
- [2] Kaaret, P., Lamb, F. K., and Swank, J. H., eds., [*X-ray Timing 2003: Rossi and Beyond*], *AIP Conf. Ser.* **714** (2004).
- [3] Kaaret, P., "Relativistic astrophysics explorer," *Adv. Space Res.* **34**, 2662 (2004).
- [4] Elvis, M., "The Extreme Physics Explorer," *Proc. SPIE* **6266**, 62660Q (2006).
- [5] Barret, D., van der Klis, M., Skinner, G. K., Staubert, R., and Stella, L., "Future X-Ray Timing Missions," *Ap. Space Sci. Suppl.* **276**, 305 (2001).
- [6] Barret, D. et al., "Science with the XEUS high time resolution spectrometer," *Proc. SPIE* **7011**, 70110E (2008).
- [7] Nath, N. R., Strohmayer, T. E., and Swank, J. H., "Bounds on Compactness for Low-Mass X-Ray Binary Neutron Stars from X-Ray Burst Oscillations," *ApJ* **564**, 353 (2002).
- [8] Bhattacharyya, S., Strohmayer, T. E., Miller, M. C., and Markwardt, C. B., "Constraints on Neutron Star Parameters from Burst Oscillation Light Curves of the Accreting Millisecond Pulsar XTE J1814–338," *ApJ* **619**, 483 (2005).
- [9] Miller, M. C., Lamb, F. K., and Psaltis, D., "Sonic-Point Model of Kilohertz Quasi-periodic Brightness Oscillations in Low-Mass X-Ray Binaries," *ApJ* **508**, 791 (1998).
- [10] Stella, L. and Vietri, M., "kHz Quasiperiodic Oscillations in Low-Mass X-Ray Binaries as Probes of General Relativity in the Strong-Field Regime," *Phys.Rev.Lett.* **82**, 17 (1999).

- [11] Poutanen, J. and Gierliński, M., “On the nature of the X-ray emission from the accreting millisecond pulsar SAX J1808.4–3658,” *MNRAS* **343**, 1301 (2003).
- [12] Psaltis, D. and Chakrabarty, D., “The Disk-Magnetosphere Interaction in the Accretion-powered Millisecond Pulsar SAX J1808.4–3658,” *ApJ* **521**, 332 (1999).
- [13] Strohmayer, T. E. and Watts, A. L., “The 2004 Hyperflare from SGR 1806–20: Further Evidence for Global Torsional Vibrations,” *ApJ* **653**, 593 (2006).
- [14] Watts, A. L. and Strohmayer, T. E., “Detection with RHESSI of High-Frequency X-Ray Oscillations in the Tail of the 2004 Hyperflare from SGR 1806–20,” *ApJ* **637**, L117 (2006).
- [15] Remillard, R. A. and McClintock, J. E., “X-Ray Properties of Black-Hole Binaries,” *ARA&A* **44**, 49 (2006).
- [16] Reynolds, C. S. and Nowak, M. A., “Fluorescent iron lines as a probe of astrophysical black hole systems,” *Phys.Rep.* **377**, 389 (2003).
- [17] Cackett, E. M. et al., “A Search for Iron Emission Lines in the Chandra X-Ray Spectra of Neutron Star Low-Mass X-Ray Binaries,” *ApJ* **690**, 1847 (2009).
- [18] Strohmayer, T. and Bildsten, L., “New views of thermonuclear bursts,” in [*Compact Stellar X-ray Sources*], Lewin, W. et al., eds., 113, New York: Cambridge University Press (2006).
- [19] Weinberg, N. N., Bildsten, L., and Schatz, H., “Exposing the Nuclear Burning Ashes of Radius Expansion Type I X-Ray Bursts,” *ApJ* **639**, 1018 (2006).
- [20] Altamirano, D., van der Klis, M., Wijnands, R., and Cumming, A., “Millihertz Oscillation Frequency Drift Predicts the Occurrence of Type I X-Ray Bursts,” *ApJ* **673**, L35 (2008).
- [21] Klein, R. I., Arons, J., Jernigan, G., and Hsu, J. J.-L., “Photon Bubble Oscillations in Accretion-powered Pulsars,” *ApJ* **457**, L85 (1996).
- [22] Jernigan, J. G., Klein, R. I., and Arons, J., “Discovery of Kilohertz Fluctuations in Centaurus X-3: Evidence for Photon Bubble Oscillations (PBO) and Turbulence in a High-Mass X-Ray Binary Pulsar,” *ApJ* **530**, 875 (2000).
- [23] Bildsten, L. et al., “Observations of Accreting Pulsars,” *ApJS* **113**, 367 (Dec. 1997).
- [24] Gavriil, F. P. and Kaspi, V. M., “Long-Term Rossi X-Ray Timing Explorer Monitoring of Anomalous X-Ray Pulsars,” *ApJ* **567**, 1067 (2002).
- [25] Kaspi, V. M., Lackey, J. R., and Chakrabarty, D., “A Glitch in an Anomalous X-Ray Pulsar,” *ApJ* **537**, L31 (2000).
- [26] Kaspi, V. M. et al., “A Major Soft Gamma Repeater-like Outburst and Rotation Glitch in the No-longer-so-anomalous X-Ray Pulsar 1E 2259+586,” *ApJ* **588**, L93–L96 (2003).
- [27] McHardy, I. M., Koerding, E., Knigge, C., Uttley, P., and Fender, R. P., “Active galactic nuclei as scaled-up Galactic black holes,” *Nature* **444**, 730 (2006).
- [28] Galloway, D. K. et al., “Thermonuclear (type-I) X-ray bursts observed by the Rossi X-ray Timing Explorer,” *ApJ Suppl.* **179**, 360 (2008).
- [29] Wen, L., Levine, A. M., Corbet, R. H. D., and Bradt, H. V., “A Systematic Search for Periodicities in RXTE ASM Data,” *ApJ Suppl.* **163**, 372 (2006).
- [30] Wolff, M. T. et al., “Eclipse Timings of the Low-Mass X-Ray Binary EXO 0748–676. III. Orbital Period Jitter Observed with the Unconventional Stellar Aspect Experiment and the Rossi X-Ray Timing Explorer,” *ApJ* **575**, 384 (2002).
- [31] Fender, R., “Jets From X-ray Binaries: A Brief Overview and Comparison with Active Galactic Nuclei,” in [*Relativistic Jets: The Common Physics of AGN, Microquasars, and Gamma-Ray Bursts*], P. A. Hughes & J. N. Bregman, ed., *AIP Conf. Ser.* **856**, 23 (2006).
- [32] van der Klis, M., “Neutron Star QPOs as Probes of Strong Gravity and Dense Matter,” in [*X-ray Timing 2003: Rossi and Beyond*], Kaaret, P., Lamb, F. K., and Swank, J. H., eds., *AIP Conf. Ser.* **714**, 371 (2004).
- [33] Atwood, W. B. et al., “The Large Area Telescope on the Fermi Gamma-Ray Space Telescope Mission,” *ApJ* **697**, 1071 (2009).
- [34] Gatti, E. and Rehak, P., “Semiconductor drift chamber — An application of a novel charge transport scheme,” *Nucl. Instr. Meth.* **225**, 608 (1984).

- [35] Oonuki, K., Inoue, H., Nakazawa, K., Mitani, T., Tanaka, T., Takahashi, T., Chen, C. M. H., Cook, W. R., and Harrison, F. A., “Development of uniform CdTe pixel detectors based on Caltech ASIC,” *Proc. SPIE* **5501**, 218 (2004).
- [36] DeGeronimo, G. et al., “Front-End ASIC for High-Resolution X-ray Spectrometers,” in [*IEEE NSS-MIC 2007, Honolulu, HI*], N03–5 (2007).
- [37] Jahoda, K. et al., “Calibration of the Rossi X-Ray Timing Explorer Proportional Counter Array,” *ApJS* **163**, 401 (2006).
- [38] Robinson, D. W., “Building a new kind of graded-Z shield for Swift’s burst alert telescope,” *Proc. SPIE* **4851**, 1374 (2003).
- [39] Agostinelli, S. et al., “Geant4-a simulation toolkit,” *Nucl. Instr. Meth. A* **506**, 250 (2003).
- [40] Opiela, J., Hillary, E., Whitlock, D. O., and Hennigan, M., [*Debris Assessment Software Version 2.0 User’s Guide*], Orbital Debris Program Office, NASA Johnson Space Center, Houston, TX (2007).
- [41] [*Taurus II User’s Manual Release 1.2*], Orbital Science Corporation (2009).
- [42] Maly, J. et al., “Hubble space telescope solar array damper,” *Proc. SPIE* **3672** (1999).